Tellus (1995), 47A, 304–323
Printed in Belgium – all rights reserved

TELLUS
ISSN 0280–6495

The impact of a digital filter finalization technique in a global data assimilation system

By LUC FILLION*, HERSCHEL L. MITCHELL, HAROLD RITCHIE and ANDREW STANIFORTH, *Direction de la Recherche en Météorologie, Service de l'Environnement Atmosphérique, 2121, route Transcanadienne, Dorval, Québec, Canada H9P 1J3*

(Manuscript received 3 March 1994; in final form 1 June 1994)

ABSTRACT

The ability of a digital filter technique to control high-frequency gravity wave noise in numerical weather forecasts based on the primitive equations is examined in the context of a global data assimilation system. The method uses a 12-h forward integration of the complete model to generate a time series that is filtered to give a balanced model state valid 6 h into the integration. This state is free of high-frequency noise and serves as a background field for the next analysis. The technique is referred to as *digital filter finalization.* The technique is first applied to a long model run in order to identify the impact of the chosen cutoff period in the design of the filter on a properly balanced model state. The robustness of the technique to typical imbalances between the mass and wind fields produced by an operational statistical interpolation procedure is also examined. Results of data assimilation experiments performed with the digital filter finalization and with the currently-operational adiabatic nonlinear normal mode initialization scheme are compared. The digital filter finalization technique examined here is shown to be an accurate, consistent and very simple way to remove the undesirable high-frequency noise from a global model forecast.

1. Introduction

Numerical weather prediction (NWP) models based on the primitive equations allow solutions with multiple time scales. If not suitably adjusted at the initial time, large-amplitude high-frequency gravity-wave noise is excited and propagates almost linearly in the domain of integration. The process of adjusting the initial conditions to avoid such imbalances is usually termed *initialization.*

The analysis component of conventional data assimilation schemes suffers from this problem which mostly stems from the fact that a proper dynamical balance for atmospheric states requires more than the first-order geostrophic assumption normally imposed on the analysis increments. In addition, these schemes generally use local (grid-point) statistical interpolation and are therefore unable to impose a coherent global balance. This results in fast gravity-wave noise with different horizontal and vertical scales superimposed on a slowly-varying meteorologically-significant state. Traditionally, these imbalances have been removed using Machenhauer's (1977) or Baer and Tribbia's (1977) nonlinear normal mode initialization (NNMI) schemes.

For regional models, the implementation of normal mode schemes is less straightforward but can be done using implicit NNMI (Temperton and Roch, 1991). Recently, Lynch and Huang (1992) and Huang and Lynch (1993) (hereinafter referred to as LH92 and HL93 respectively) introduced a digital-filter technique to initialize forecasts produced with HIRLAM (High-Resolution Limited-Area Model). Their technique was shown to efficiently remove gravity-wave noise in their

* Corresponding author address: Dr. Luc Fillion, Direction de la Recherche en Météorologie, Service de l'Environnement Atmosphérique, 5e étage, 2121 route Transcanadienne, Dorval, Québec, Canada H9P 1J3.

forecast, was easy to implement, incorporated all physical processes, and performed better than their NNMI scheme.

Recent work on three and four-dimensional variational data assimilation schemes (3DVAR and 4DVAR) has shown that higher-order balance constraints can be incorporated into the analysis step itself (Courtier and Talagrand, 1990; Thépaut and Courtier, 1991; Thépaut et al., 1993). At the US National Meteorological Center (NMC) a 3D variational analysis scheme, termed Spectral Statistical Interpolation (SSI), has been operational since June 1991 (Parrish and Derber, 1992). The SSI is a spectral rather than local (grid-point) statistical interpolation procedure, and uses a simple linear-balance relationship for analysing geostrophic increments to a "balanced" (noise-free) background model state while also allowing an ageostrophic component. Analyses produced by the SSI scheme are apparently free of significant gravity-wave noise, which eliminates the need for an initialization step. The same ideas of normal mode balance as those used in present operational data assimilation systems are being tested in other variational analysis schemes currently under development. Due to the relatively-recent introduction of the digital filter technique, its usefulness in 3D or 4DVAR remains an open question, although a preliminary study in the context of 4DVAR was reported in Gustafsson (1992).

Our objective in this study is to examine the digital-filter approach in a wider context than LH92/HL93 in order to better evaluate its potential usefulness and possible limitations in present and future data assimilation schemes. This is accomplished by first testing the *accuracy* of a digital-filter scheme (to be described in Section 2) on a balanced model state. Although "balance" is reasonably definable at some scale (Errico, 1989), it is difficult to precisely define it in a complex diabatically-forced model such as that of the present study. We therefore adopt the general approach of Errico to characterize the control "balanced" state as that resulting from a long run of the model. To the extent that our model establishes a reasonable dynamical and physical balance, a "balanced" state is defined to be the result of a long model integration. Secondly, the *robustness* of the method is examined in the context of typical imbalances present in operational analysis fields. This is done in the context of present-day global data assimilation schemes based on statistical interpolation. The essential results that demonstrate the performance of the digital-filter in a global data assimilation system will be presented. Due to its wide use in NWP, Machenhauer's NNMI scheme will be used as a basis of comparison.

Section 2 describes the general methodology and, in particuliar, the digital filter finalization that we have examined. In Section 3, results are presented for three different aspects concerning the impact of the digital filter (a) on a balanced model state, (b) on an uninitialized operational analysis, and (c) in a global data assimilation scheme. The conclusions of the study are presented in Section 4.

2. Methodology

2.1. The model and data assimilation system

The forecast model used in this study is the version of the global primitive-equations spectral model employed operationally at the Canadian Meteorological Centre (CMC) from March 1991 until June 1993 when its horizontal resolution was increased in conjunction with several other modifications. The model uses a semi-implicit semi-Lagrangian time integration scheme as described in Ritchie (1991), and combines the spectral (spherical harmonic) method in the horizontal with the finite-element method in the vertical. A triangular truncation at wavenumber 79 (T79) is used, with 21 σ-levels in the vertical (i.e., $\sigma = p/p_s$ where p is pressure and p_s is the surface pressure), and a 30-min timestep. As summarized in Girard et al. (1991), the physical parameterization includes a planetary boundary layer, a surface layer, solar and infrared radiation, large-scale precipitation, moist convection and gravity-wave drag. A complete description of the operational global data assimilation system can be found in Mitchell et al. (1993). Fig. 1 of that paper shows the vertical distribution of the model and analysis levels.

2.2. The time-filtering procedure

Our use of a digital filter differs from that of Lynch and Huang (LH92, HL93) and can be summarized as follows. In currently-operational intermittent data assimilation systems, a balanced model state which serves as a background field is required at the analysis time. This state typically comes from a 6-h integration of the model starting from initialized initial conditions using the NNMI procedure. An alternate way of producing a model state free of gravity-wave noise at the analysis time is simply to perform a 12-h forward integration to generate a time series of forecast variables that are then filtered with a centered digital filter. This integration uses all the physical processes normally included in forecast mode and no NNMI initialization is applied at the initial time. It has the potential advantage when compared to the LH92 and HL93 schemes of avoiding the need to integrate the model *adiabatically* backwards in time. This allows diabatic effects to be treated more consistently.

In this study, the filter is applied to all predictive variables of the model. The latter uses a half-hour timestep which gives an operationally-feasible implementation with a 25-point time series. The filtered central estimate is thus valid 6 h after the previous analysis time and should provide a noise-free background field for the current analysis time. During the integration of the model, the time sequence of model variables are generated and may be represented as

$$\{X_0, X_{\Delta t}, X_{2\Delta t}, ..., X_{M\Delta t/2}, ..., X_{M\Delta t}\},$$

where M is the total number of timesteps (24 here) starting from the original (uninitialized) analysis at time zero. A relabeling of the time series as

$$\{X_{-N}, X_{-N+1}, ..., X_0, X_1, ..., X_N\},$$

where $N=M/2$, defines the initial time as index $-N$ and the central time (the 6-h forecast) as index zero. Following LH92, a Heaviside (unit-step) function is used in Fourier space to eliminate the small periods (high-frequencies) of the signal. The discrete form of the convolution which performs the time filtering is represented as

$$X_0^{\mathrm{f}} = \sum_{k=-N}^{N} h_k X_k.$$

The digital filter coefficients are defined as

$$h_k = \frac{\sin k\theta_{\mathrm{c}}}{k\pi}, \qquad \theta_{\mathrm{c}} = \frac{2\pi\,\Delta t}{T_{\mathrm{c}}},$$

where T_{c} is the cutoff period and θ_{c} the digital frequency at T_{c}. As in LH92, a Lanczos window is used to reduce the Gibbs oscillations due to the use of a truncated Fourier series, i.e., each coefficient of the filter is multiplied by

$$\omega_k = \frac{\sin\left(\dfrac{k\pi}{N+1}\right)}{\left(\dfrac{k\pi}{N+1}\right)}.$$

The associated transfer function $H(\theta)$ (i.e., the function by which a pure sinusoidal oscillation is multiplied when subjected to the filter) is

$$H(\theta) = \sum_{k=-N}^{N} h_k \mathrm{e}^{-ik\theta} = h_0 + 2\sum_{k=1}^{N} h_k \cos k\theta.$$

Practically, the filter coefficients are computed prior to the integration and the sum is accumulated in a workspace vector of the same dimension as the model-state vector to produce the filtered estimate valid 6 h after the initial time. Fig. 1 shows the digital filter coefficients and transfer function (including the windowing) for the 8-h and 6-h cutoff periods (solid lines and dashed lines, respectively) used for the experiments to be described in the following section. For both cutoff periods, it is seen that during the first two hours of integration, the filter has relatively small coefficients. This period is short with respect to the nonlinear quasi-geostrophic adjustment process but is significant for moisture adjustment outside the tropics (see Huang and Sundqvist, 1993, for instance). Since the filter acts symmetrically about the time of validity of the background field (i.e., 6 h), the phase of each Fourier component of the signal is unaffected by the filter. The use of a 12-h time span for the time series is well above the minimum time span based on the uncertainty principle (Hamming, 1989; HL93) with an 8-h cutoff period, which is about 4 h.

As is usually observed from time series of model variables produced from a forecast initiated with unbalanced initial conditions (e.g., an analysis coming from a statistical interpolation procedure), the gravity-wave noise appears with periods less than about 8 h (see, e.g., Section 3). With regard to this aspect, the 8-h cutoff period is preferable to the 6-h one (see Fig. 1) in that it more strongly damps the high-frequency noise. On the other hand, a

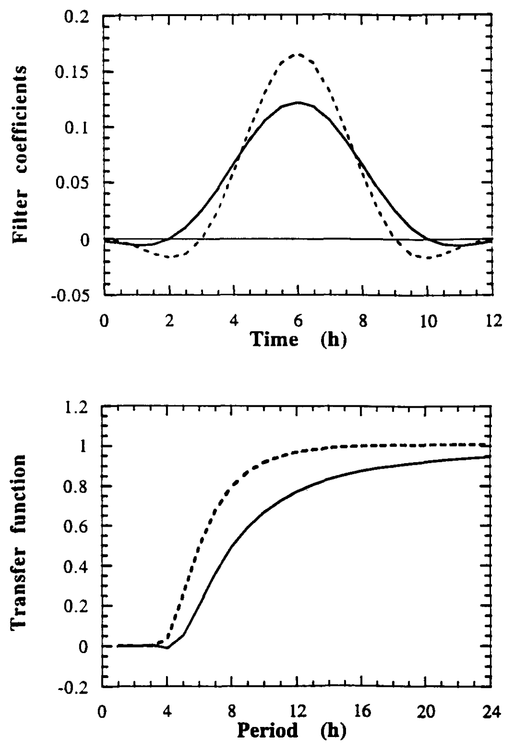

Fig. 1. Digital-filter coefficients (top) and transfer function (bottom) for a 12-h forecast with a 30-min timestep. Dashed line: 6-h cutoff period. Solid line: 8-h cutoff period. Lanczos windowing is used.

dominant semi-diurnal signal is developed (with maximum amplitude in the tropics) by a balanced model forecast and to preserve that signal a response as close to unity as possible is required around the 12-h period. In this respect, the 6-h cutoff period is preferable to the 8-h one, the transfer function at 12 h being 0.97 instead of 0.77. The impact of these digital filter specifications on a balanced model state and within a data assimilation cycle will be examined in the next section. For both NNMI and digital filter schemes, it must be stressed that an appropriate cutoff period has to be determined by considering the overall effect of the scheme in an analysis-initialization (finalization) cycle.

The procedure described above is referred to in the remaining text as "digital-filter finalization" (DFF). The term "finalization" is borrowed from Temperton and Williamson's (1979) report on the use of Machenhauer's NNMI scheme applied at the end of the 6-h forecast. They found little difference upon applying Machenhauer's scheme at the beginning (initialization) or at the end (finalization) of a 6-h forecast. While Temperton and Williamson used the term "finalization" to refer to a procedure applied only to the final 6-h forecast, the term as used here with the digital-filter involves using the entire 12-h time series to produce the 6-h filtered forecast. With this important distinction in mind, we will loosely refer to our procedure as a finalization procedure in the remaining text. We note that the time-averaging scheme proposed by Edelmann (1972) also involved producing a forecast out to time $M\,\Delta t$ in order to produce a balanced state at time $M\,\Delta t/2$.

2.3. *Construction of a balanced model state*

The forecast that serves as "truth" for defining a balanced state includes all physical processes and results from a long model integration. The initial conditions for this integration are the σ-surface analyses obtained from the operational data assimilation cycle valid at 12 UTC 1 August 1991. The digital filter is applied during the last 12 h of a 10-day + 12-h control forecast (without any intervening restart procedure), thus providing a filtered state at time $t = 10$ day + 6 h, i.e., 18 UTC 11 August 1991 (hereinafter referred to as time τ). No other NNMI or DFF was used in any of the long integrations required by the control or DFF experiments, thereby permitting the model to dynamically determine its balanced state.

2.4. *Basis of comparison with the NNMI scheme*

Some comparisons will be made with the currently-operational initialization scheme at CMC, which is an adiabatic explicit Machenhauer NNMI scheme. The basic set of equations (resulting from the Eulerian form of the primitive equations) used to derive the vertical and horizontal normal modes used in the NNMI scheme can be found in Staniforth and Daley (1977) and Béland and Beaudoin (1985). The procedure used to compute the horizontal normal modes has been described by Temperton (1989). The equations are linearized about a basic state at rest having an isothermal temperature profile $T^* = 300$ K. The vertical discretization used to solve the vertical structure equation is by linear finite-elements and we give in Table 1 the complete set of 21

Table 1. *Values of sigma levels of the model together with the equivalent depths H_n based on an isothermal vertical temperature profile of $T^* = 300$ K*

n	H_n (m)	σ
1	11679.25	0.010
2	2941.54	0.045
3	1032.00	0.090
4	469.02	0.140
5	248.38	0.190
6	142.47	0.245
7	86.53	0.304
8	54.67	0.366
9	35.97	0.430
10	24.53	0.494
11	17.16	0.558
12	12.18	0.622
13	8.68	0.684
14	6.13	0.744
15	4.30	0.800
16	2.96	0.850
17	1.98	0.894
18	1.22	0.932
19	0.68	0.964
20	0.32	0.990
21	0.05	1.000

equivalent depths and σ-levels, where H_n is the nth equivalent depth of the model. Three iterations of Machenhauer's adiabatic NNMI scheme are used for the initialization of the first three vertical modes. The limiting period to select the gravity modes to be initialized is set at 8 h, as in the currently-operational version.

No physical processes are included in the computation of the local time tendencies required by the initialization scheme. These local time tendencies are computed using an Eulerian formulation which dates back to an earlier version of the model. With regard to the absence of diabatic effects in the NNMI scheme used here, we argue, in light of extensive studies by Errico (1984), Errico and Rasch (1988; hereinafter referred to as ER), Errico et al. (1988; hereinafter EBG) and Errico (1989), that our initialization results *with an 8-h cutoff period* would not be significantly altered if diabatic effects were considered. Diabatic balance makes sense, however, for some gravity modes with larger natural periods such as, e.g., tidal oscillations (Wergen, 1989) and large-scale zonally symmetric gravity modes with periods greater than 35 h (Gelaro and Errico, 1993). Some shortcomings of adiabatic NNMI with a 24-h cutoff are illustrated in the Appendix.

3. Results

3.1. Impact on a dynamically-balanced model state

Attention is focused here on the impact of the DFF scheme when applied to a balanced model state produced by a long-term model integration. For Machenhauer's NNMI scheme, the work of Errico and his collaborators mentioned above gives a fairly-detailed analysis of the nature of balance in NWP and climate models in terms of various temporal and spatial scales, the presence or absence of physical terms in the balance condition, and finally the various orders of Machenhauer's balance condition itself. Here, we look simply at the impact of a single application of the DFF scheme starting with already-balanced initial conditions. As in ER, we examine quantities which may be modified by an initialization scheme, such as: the zonal-mean meridional mass streamfunction, the amplitude of the divergent wind and the surface pressure field.

The impact of the DFF scheme on the zonal-mean meridional mass streamfunction, which is closely associated with the Hadley circulation, is first examined. The result of the DFF scheme is valid at time τ (as defined in Subsection 2.3) and results from the time series of model variables for a 12-h period beginning at day 10. Fig. 2 shows the *changes* to the meridional streamfunction of the control integration at time τ due to NNMI-8 h (upper panel) and DFF-8 h (lower panel). *Use of the DFF procedure results in a reduction of the changes by an order of magnitude* as compared to NNMI: note that the contour interval for the lower panel is a factor of 10 smaller than for the upper panel. Thus the DFF procedure results in an atmosphere that is much closer to that determined dynamically than does adiabatic NNMI. The much larger changes due to applying the NNMI scheme with a 24-h cutoff period are discussed in the *Appendix*. The meridional circulation is further discussed later in this section.

A measure of the strength of the divergent circulation is given by

$$V_\mathrm{d} = (u_\mathrm{d}^2 + v_\mathrm{d}^2)^{1/2}.$$

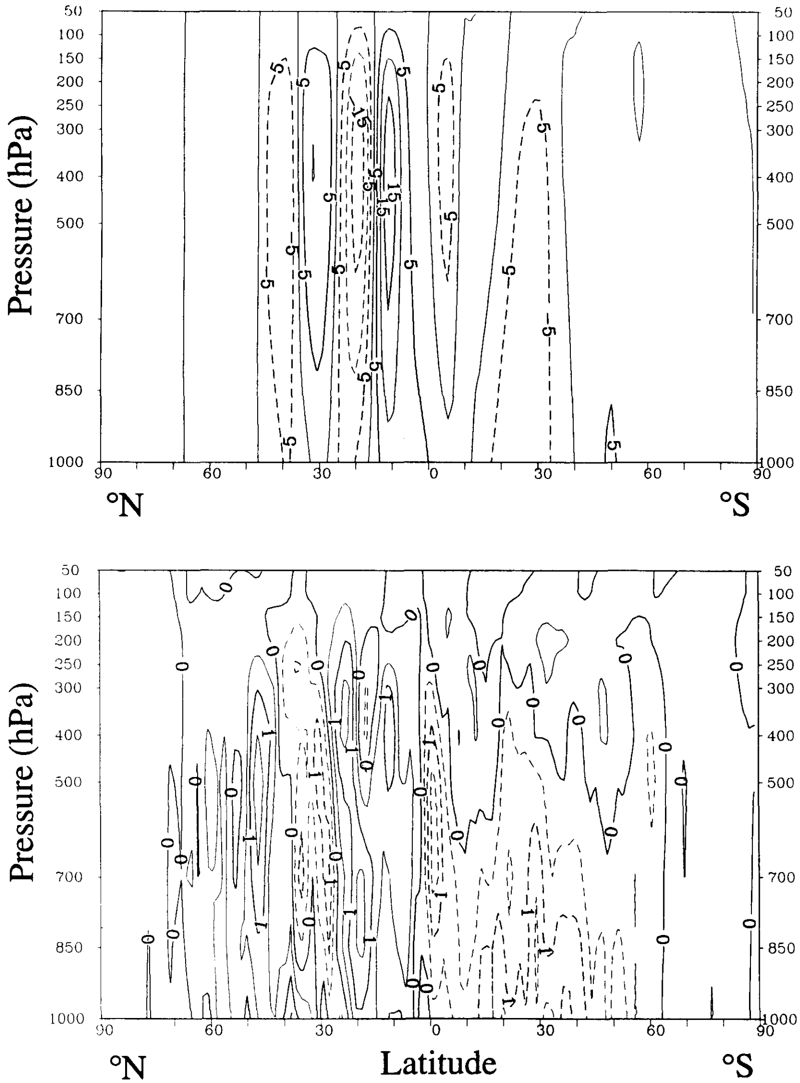

Fig. 2. Changes to the meridional streamfunction of the control integration at time $t = \tau$. Upper panel: due to the NNMI-8 h scheme, contour interval 5×10^9 kg s^{-1}. Lower panel: due to the DFF-8 h scheme, contour interval 0.5×10^9 kg s^{-1}.

A time sequence of V_d every 12 h during the 10-day integration of the model (not shown) indicates that the strength of the divergent wind field (i.e., values greater than 10 m s^{-1}) is established during the first day of integration and can be associated with the so-called spin-up time. The NNMI-8h and the DFF-8 h schemes produce changes of less than 0.2 and 0.05 m s^{-1} respectively, *i.e., with this cutoff period, both the NNMI and DFF schemes have negligible impact, with the impact of the DFF scheme on a dynamically-balanced field being 4 times smaller*. Again, as discussed in the Appendix, the NNMI scheme with a 24-h cutoff period has a much larger impact.

We now examine the impact of the DFF scheme on the thermal tides. Wergen (1989) showed that

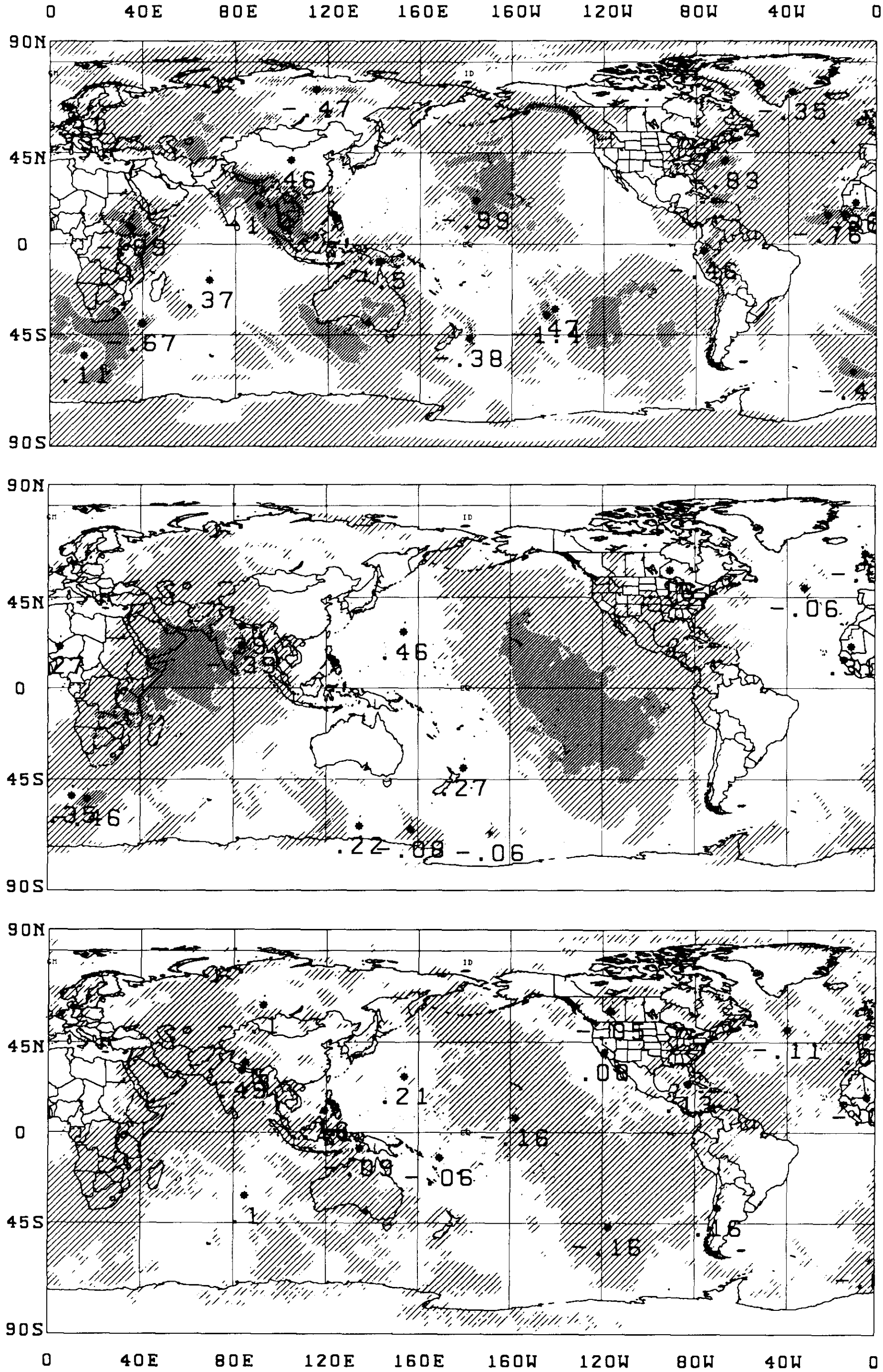

Fig. 3. Surface pressure changes (hPa) to the control fields at time $t = \tau$. Upper panel: using the NNMI-8 h scheme; middle panel: using the DFF-8 h scheme, and lower panel: using the DFF-6 h scheme. Light stippling is associated with values between 0 and -0.2 hPa, and heavy stippling with values less than -0.2 hPa.

the standard algorithm of Machenhauer could be simply modified to take into account the specific balance of the atmospheric tides. Ballish et al. (1992; hereinafter referred to as BAL92) developed an incremental NNMI scheme where the gravity mode time-tendency of the initialized analysis is forced towards the gravity mode time-tendency of the background field. That scheme was shown to successfully maintain a realistic equilibrium of the forecast tidal oscillations, whose quality was demonstrated by examining the time-mean analysis increments of the large zonal scales (wavenumbers 0–2). We examine here the effect of Machenhauer's NNMI and the DFF scheme on a balanced surface pressure field. The results to be discussed agree with those of BAL92 concerning the time before which a clear thermal-tide signal can be observed, i.e., no clearly identifiable tidal pattern could be observed if the control integration was shorter than 2 days. This is attributable to the initial spin-up of the tides.

Fig. 3 shows the surface-pressure changes (hPa) at time τ due to NNMI-8-h (upper panel), DFF-8-h (middle panel) and also DFF-6-h (lower panel). The amplitude of the changes for the DFF-8-h scheme is less than for the NNMI-8-h case with a maximum in the tropics of 0.46 hPa as compared to 1.4 hPa for the latter and exhibits changes of the semi-diurnal type shown in BAL92 (their Fig. 1). The amplitude of this zonal wavenumber two pattern is further reduced by a factor of 2 when a DFF-6-h scheme is used (lower panel). The changes with the NNMI-8-h scheme are of larger amplitude and do not exhibit this coherent zonal wavenumber two pattern.

The impact on the tidal oscillations can also be examined in Fig. 4, which shows the 48-h time-trace of surface pressure for a point located in the

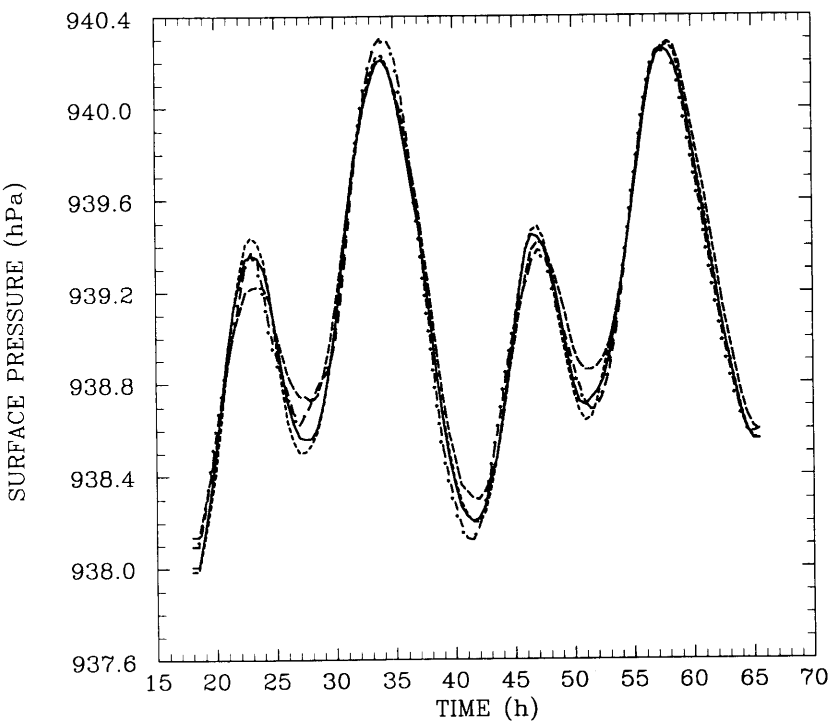

Fig. 4. Time traces of surface pressure for a point located at (0° W, 30.6° N) for 48-h forecasts beginning at time τ. The solid line is from uninitialized balanced initial conditions. The dash-dotted line is from initialized initial conditions using the NNMI-8 h scheme and the short (long)-dashed line is from digitally finalized initial conditions using the DFF-6-h (8-h) scheme.

tropics beginning with balanced initial conditions valid at time τ. Both NNMI and DFF schemes with these reduced cutoff periods are seen to maintain the dominant semi-diurnal and diurnal oscillations present in the control integration. By contrast, adiabatic NNMI with a 24-h cutoff period largely eliminates the tidal oscillation, as discussed in the Appendix.

In summary, with either an 8-h or 6-h cutoff the DFF technique has negligible impact on a balanced model state. The atmospheric tide is also well maintained but with a smaller amplitude than the control for the 8-h cutoff period. The DFF-6 h does better due to a larger response at the dominant semi-diurnal period. The adiabatic NNMI-8-h scheme produces results comparable to the DFF schemes but has a significant impact on the zonal-mean meridional mass streamfunc-

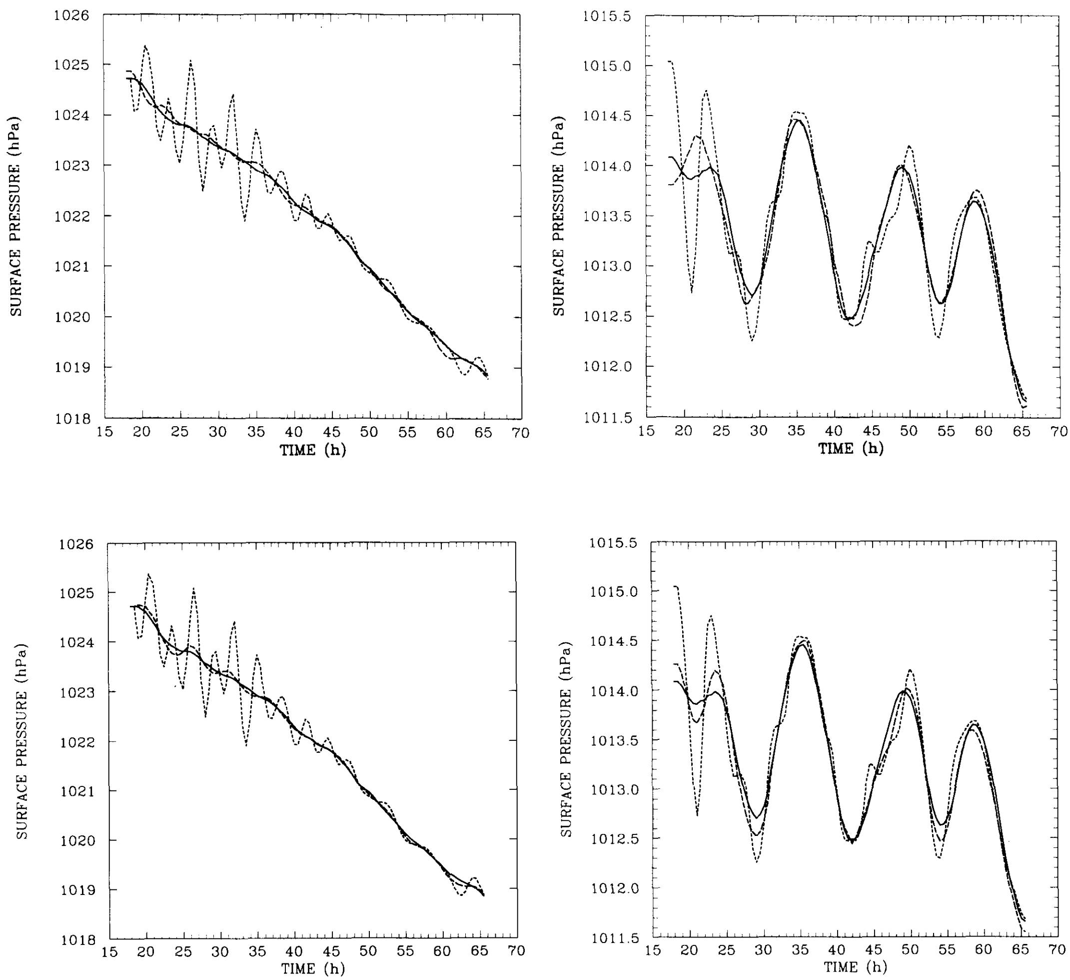

Fig. 5. Time traces of surface pressure for 48-h forecasts for points located at (0° W, 68° N) (left) and (0° W, 0.75° N) (right). In all panels, the short-dashed line is from uninitialized initial conditions, while the solid line is from digitally finalized initial conditions using the DFF-8-h scheme. In the upper panel, the long-dashed line is from initialized initial conditions using the NNMI-8-h scheme. In the lower panel, the long-dashed line is from digitally finalized initial conditions using the DFF-6-h scheme.

tion whereas the DFF scheme performs better, i.e., produces changes that are an order of magnitude smaller.

3.2. *Impact on an uninitialized analysis*

We now examine the impact of the DFF scheme in a more realistic context in which the initial imbalance between the mass and wind fields resulting from the operational statistical interpolation analysis scheme gives rise to unrealistic, large amplitude, gravity-wave noise. Fig. 5 shows the time traces of the surface pressure during the first 2 days of integration for a winter case beginning at 18 UTC 2 February 1991 for two points located respectively at (0°W, 68°N) (left) and (0°W, 0.75°N) (right). In all panels, the short-dashed curve is from an uninitialized integration beginning with initial conditions on σ-levels valid at 18 UTC. These initial conditions were produced by an uninitialized 6-h model run from the σ-level operational analysis valid at 12 UTC. In all panels, the solid curve is from balanced initial conditions produced with the DFF-8 h scheme starting at 12 UTC. We consider first the upper panels where the long-dashed curve is from balanced initial conditions using the NNMI-8 h scheme applied at 18 UTC on the uninitialized 6-h forecast mentioned previously. The results are typical of those obtained with other cases and show that the DFF-8 h scheme effectively removes the high-frequency noise in the forecast. The structure of the vertical motion field resulting from the two schemes was almost identical. The lower panels of Fig. 5 show that the use of a DFF-6 h scheme (long-dashed curve) leaves more amplitude in the noise with about a 6-h period than the DFF-8-h scheme (solid curve), consistent with the shape of the transfer function of Fig. 1. Note that in all cases, the tropical point exhibits no semi-diurnal oscillation during the first 12 h of integration since the initial conditions came from the global analysis produced by a data assimilation system which used an adiabatic NNMI scheme with a 24-h limiting period. As discussed in the Appendix, this initialization eliminates this type of oscillation during the first 15–20 h of integration.

One significant difference was observed between the results for a global model of the DFF and NNMI schemes as used here and the corresponding results of LH92 (see their Fig. 5) and HL93 (Fig. 5) for a limited-area model. The difference concerns the surface pressure tendencies resulting from the application of NNMI and DFF schemes to a typical uninitialized analysis produced by the data assimilation scheme. To ensure a proper comparison with the DFF scheme, a nonlinear normal mode *finalization* (NNMF) is used to examine this point. Fig. 6 (upper panel) shows the surface pressure tendency (hPa/3 h) resulting from NNMF applied at the end of a 6-h forecast starting from the uninitialized operational analysis valid at 12 UTC 2 February 1991. For clarity, only moderate to strong falling surface pressures are shown (but the same conclusion applies to weak values). As one would expect, there is a good relationship between the regions of rising and falling surface pressures and the position and displacement of the synoptic patterns. These features are particularly meaningful over the province of Québec, where the rapidly falling pressure ahead of the trough is very well delimited on the western side by the trough axis. Very small (insignificant) differences were obtained when the surface pressure tendencies were computed from a 6-h forecast *initialized* at the analysis time with NNMI. Moreover, surface pressure tendencies computed at the initial time, immediately after applying NNMI at the analysis time exhibit the same type of synoptic coherence (result not shown). The lower panel of Fig. 6 is the result of applying the DFF-8 h scheme starting with the same initial analysis as for the NNMF case. It shows a close resemblance with the upper panel, and it can be concluded that both schemes produce acceptable synoptic results. Although only the North-American region is presented, this conclusion applies equally well elsewhere.

These results may be contrasted with those of LH92 and HL93 who found a clear superiority of the digital filter initialization over the NNMI scheme when comparing balanced surface pressure tendencies for instance. This apparent failure of Machenhauer's NNMI scheme for the HIRLAM model seems to be related to the problem of properly specifying consistent lateral boundary conditions for the mass and wind field adjustments for a limited area model, as discussed in Section 1. This is supported by the fact that the largest contribution to the noise in the surface pressure tendencies originates from analysis imbalances present in the external mode, for which Machenhauer's scheme is known to be a good approxima-

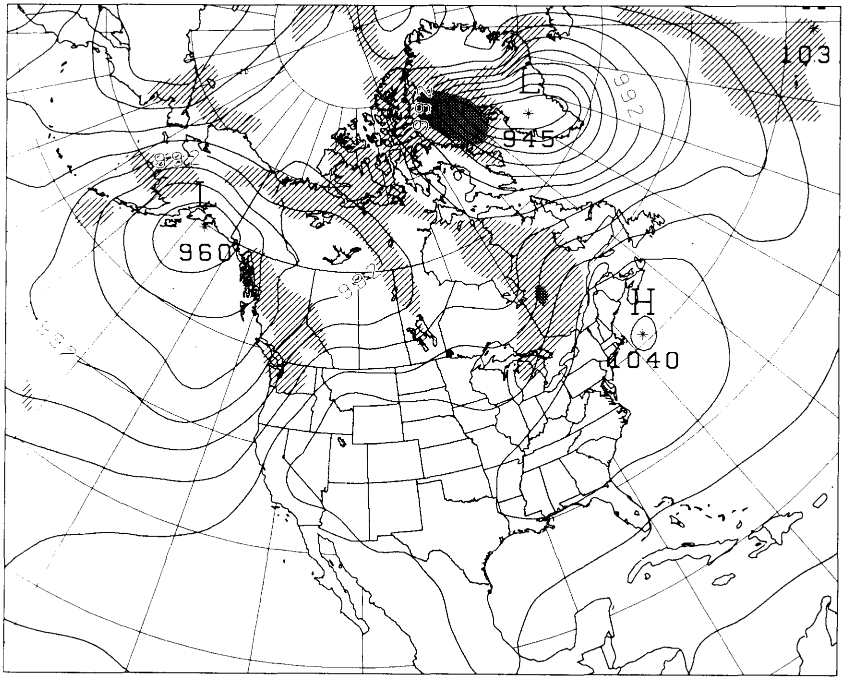

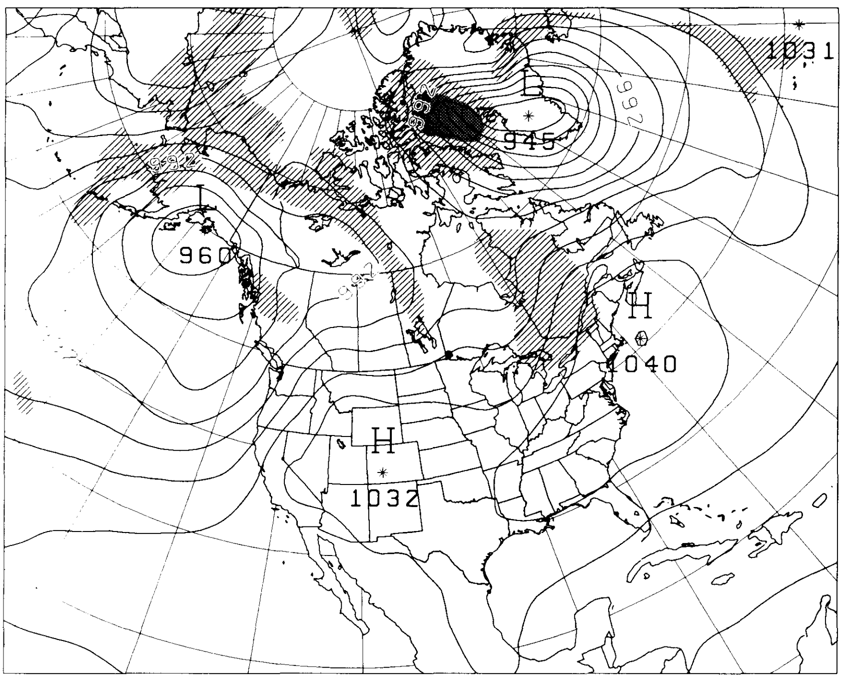

Fig. 6. Initial surface pressure tendency (hPa/3 h) for initial conditions prepared with the NNMF-8-h scheme (top) and the DFF-8-h scheme (bottom). For clarity, only falling surface pressures are shown. Light stippling is associated with values greater than 2 hPa/3 h, and heavy stippling with values greater than 6 hPa/3 h.

tion to a model's balance. Also, results of the type reported by LH92 and HL93 with Machenhauer's NNMI scheme may differ for other regional models. For instance, Errico (personnal communication) examined the surface pressure tendencies resulting from the implicit Machenhauer's NNMI scheme for the NCAR (National Center for Atmospheric Research) regional mesoscale model (an updated version of the MM4 described in Errico and Bates, 1988). Results similar to those reported here (Fig. 6) were found.

It is worth commenting on some aspects of the application of normal mode schemes to the HIRLAM and other regional models. For such models, explicit NNMI is complicated by both the non-separability of the linearized dynamical equations and also by details of the specification of the model boundary conditions. This latter aspect renders the normal mode method difficult to apply even for implicit schemes (Temperton, 1988) where, for instance, the construction of orthogonal fast (gravity) and slow (Rossby) subspaces or simply achieving consistency between mass and wind field adjustments at the boundaries is difficult. Despite this latter problem, substantial noise reduction can be accomplished (Bourke and McGregor, 1983; Errico and Bates, 1988; Juvanon-du-Vachat, 1992; Bijlsma and Hafkenscheid, 1986: see also the approach of Browning and Kreiss, 1982 for open-boundary models). The inherent limitation of both the explicit and implicit normal-mode method for *nested* regional models can be circumvented, however, by adopting a *variable-resolution* model (Temperton and Roch, 1991; Côté et al., 1993).

3.3. *Impact in a global data assimilation cycle*

So far it has been shown that the DFF scheme has a negligible impact on a state already in dynamic balance and can also successfully suppress the high-frequency temporal noise in a model forecast starting from a realistic analysis. In a general sense, imbalances not only excite high-frequency gravity waves but also contribute to the generation of false low-frequency gravity (and Rossby) waves (spurious convection in the tropics represents such a source of imbalance). Since 6 and 8 h are rather low values of the cutoff period, it remains to examine the impact, within a sequential data assimilation cycle, of not initializing the analyzed gravity modes which have larger natural periods.

For purposes of comparison, four data assimilation cycles were performed in all, two with the NNMI scheme using 24- and 8-h cutoff periods and two using the DFF scheme with 8- and 6-h cutoff periods. The initial conditions for the experiment consisted of the global analyses on σ-surfaces for 12 UTC 16 March 1993 obtained from the CMC operational global data assimilation cycle. All data assimilation cycles were run for a two-week period and statistics measuring the differences between (i) the analyses and radiosonde observations, and (ii) the 6-h forecasts (background fields) and these radiosonde observations, were accumulated.

The evaluations of the analyses and 6-h forecasts against North-American radiosondes revealed insignificant differences in performance for all data assimilation experiments (including the NNMI-24-h case), i.e., differences of less than 1.5 m for geopotential height and less than 0.2 m s^{-1} for both wind components. The results from the DFF-8 h scheme were slightly, but systematically, better than the other three cases. The same conclusion applies to the evaluations against tropical radiosondes (i.e., those within 30° of the equator). It is interesting that this type of evaluation against radiosonde data was unable to discriminate between the various schemes.

The similarities and weaknesses of the NNMI and DFF procedures in the tropics can be detected by examining the results in terms of the time-averaged increments of the three components of the data assimilation system (forecast (ΔF), analysis (ΔA), and initialization (ΔI)) at 12 UTC for the last week of the assimilation cycles. Fig. 7 shows the zonal-mean meridional mass streamfunction computed from the quantities ΔF, ΔA and ΔI for the data assimilation experiment which used the NNMI-8-h scheme. It is first seen that the relationship $\Delta F > \Delta A > \Delta I$, discussed by Hollingsworth et al. (1986) and Mitchell et al. (1993) in the context of operational data assimilation is satisfied here by the zonal-mean meridional mass streamfunction. Note that this result was expected a priori for ΔF and ΔI but also applies for ΔA. A similar procedure was used to compute ΔF for the DFF-8 h and DFF-6-h data assimilation experiments. In that case, differences between the 6-h finalized background fields and the *unini-*

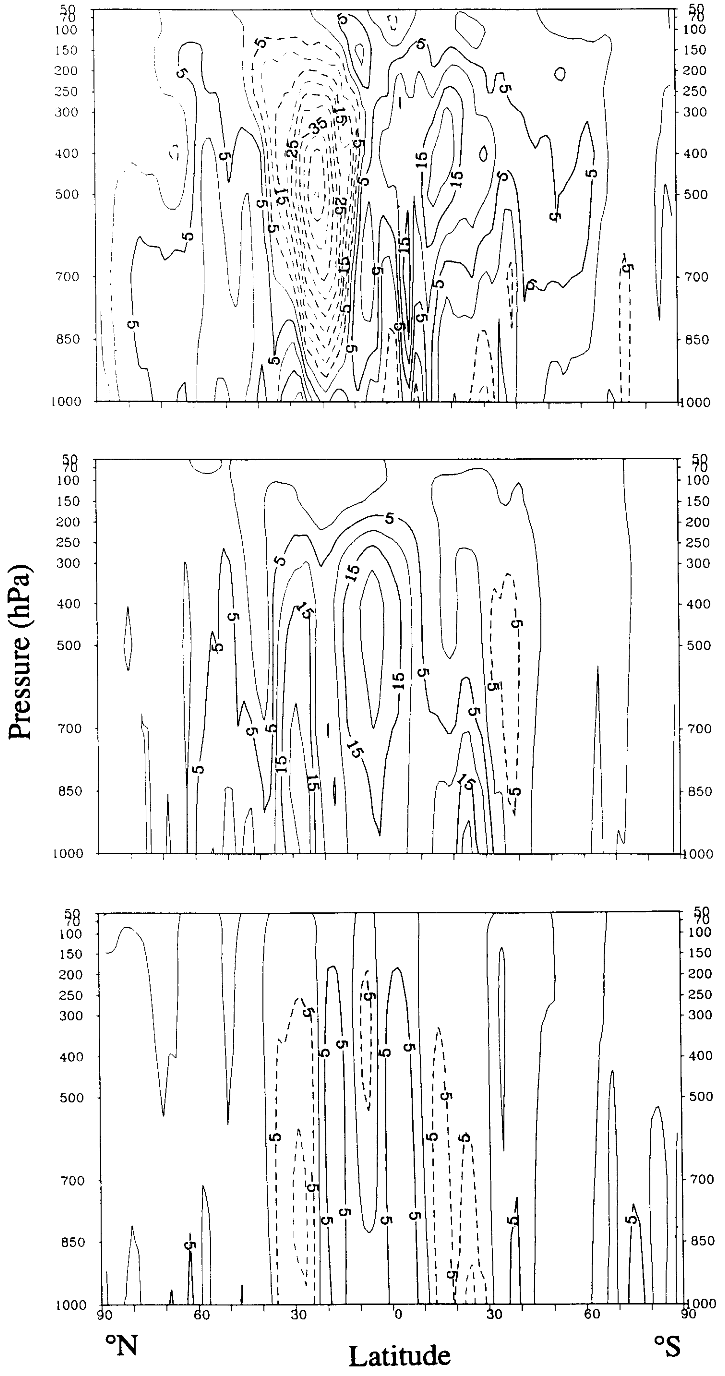

Fig. 7. The 1200 UTC 24 March–30 March 1993 time-averaged changes to the meridional circulation due to forecast (top), analysis (middle), and initialization (bottom) of the data assimilation experiment using the NNMI-8-h scheme. Contours are in units of 5×10^9 kg s^{-1}.

tialized analyses were used to produce fields of ΔF. The zonal-mean meridional mass streamfunctions computed from these ΔF (not shown) showed insignificant differences as compared to the NNMI-8 h results of the upper panel of Fig. 7.

The quantity ΔA for the DFF-8-h scheme is shown in Fig. 8. These changes are very close to the results of the NNMI-8-h scheme (Fig. 7 middle panel) but are slightly smaller. The corresponding results for the DFF-6-h scheme (not shown) are very similar, although slightly larger in the tropics. Thus the DFF-8-h (6-h) and NNMI-8-h schemes produce very similar results in a global data assimilation procedure, with the DFF-8 h scheme producing the smallest analysis changes. When a 24-h cutoff was used for the NNMI, the three components of the data assimilation cycle produced changes of the same order of magnitude in the zonal-mean meridional mass streamfunction in the tropics, with ΔA and ΔI dominating ΔF in some regions, as in Mitchell et al. (1993, Fig. 11).

We now examine the impact of the initialization procedures on the thermal tides. As discussed for instance by ER and EBG, the validity of the diabatic Machenhauer NNMI scheme is questionable in the tropics when judged with respect to a long-term model forecast. That is, since the predominant tropical modes have natural periods which are similar to the time scales of the various processes which force the modes, the neglect of the time-tendency of the gravity modes as compared to other terms in the prognostic equations is unjustified. By requiring the time-tendencies of the initialized modes to be close to the time-tendency of the background field, the incremental NNMI procedure of BAL92 was found to produce analysis increments with no apparent tidal mode problems (especially with regard to the semidiurnal oscillation). By contrast, the scheme of Wergen (1989) uses a time history to estimate the time-tendency of the tidal modes. Here, since the digital filter has a response close to unity at 12 h, we ensure that the model-developed tidal oscillation is maintained during the data assimilation period.

This expectation is confirmed in Fig. 9 where three surface pressure forecasts are compared with observed data at station Kaolack (14° N, 16° W) during a 2-day period. The thin solid curve (with circles) indicates the surface pressure reported every 6 h by the station. The heavy solid curve is the forecast, at 6-h intervals, from digitally finalized initial conditions valid at 18 UTC 24 March 1993. These initial conditions were produced by taking the uninitialized analysis on σ-surfaces valid at 12 UTC 24 March 1993 from the DFF-6-h data assimilation cycle, integrating

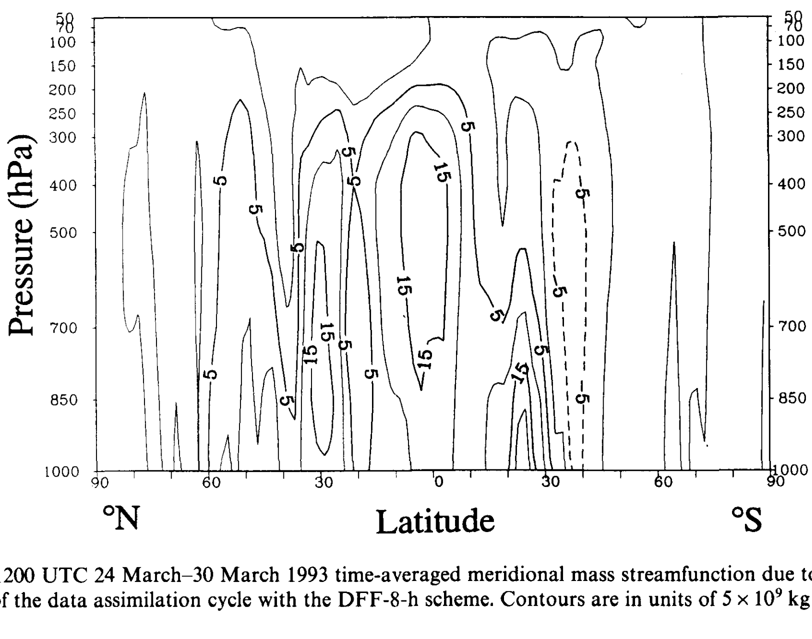

Fig. 8. The 1200 UTC 24 March–30 March 1993 time-averaged meridional mass streamfunction due to the analysis increments of the data assimilation cycle with the DFF-8-h scheme. Contours are in units of 5×10^9 kg s^{-1}.

for 12 h and then digitally filtering the resulting time series. This corresponds to the procedure that could be used operationally to make a forecast. The analogous procedure using the NNMI-8 h scheme is to take the background field on σ-surfaces produced by the NNMI-8 h data assimilation cycle, valid at 18 UTC 24 March 1993, and make a forecast. Note that, as with the DFF-6-h forecast, no data after 12 UTC are used to produce this forecast, which is plotted as the heavy dashed curve in Fig. 9. Both DFF-6-h and NNMI-8-h schemes are seen to produce a realistic semi-diurnal oscillation which is well developed right at the beginning of the forecast (i.e., with no apparent spin-up problem) and closely approximate the observed signal. Note that the phases of the signals of the three curves are identical. The overall behavior of the DFF-6 h forecast appears somewhat better than the NNMI-8-h case and is comparable in accuracy to the results presented by Wergen (1987) and BAL92 with their improved NNMI schemes. The results with the DFF-8-h scheme (the thin dashed-curve) indicate that the semi-diurnal oscillation is less developed during the first 15 h of integration (and presumably therefore also during the data assimilation cycle). Consequently, the DFF scheme performs better with a 6-h cutoff than an 8-h cutoff in this regard, consistent with its improved transfer coefficient at 12 h.

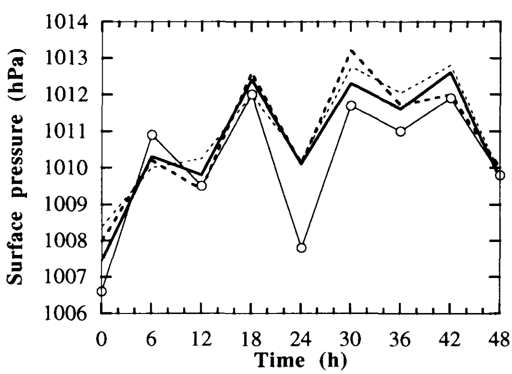

Fig. 9. Surface pressure at Kaolack (14° N, 16° W) from 18 UTC 24 March to 18 UTC 26 March 1993. Thin solid line with circles: observed. Heavy solid curve: forecast beginning with digitally finalized initial conditions produced with a DFF-6-h scheme starting from sigma analysis taken from the DFF-6-h data assimilation cycle and valid at 12 UTC. Heavy dashed curve: forecast from initialized initial conditions with a NNMI-8-h scheme valid at 18 UTC and extracted from the NNMI-8-h data assimilation cycle. Thin dashed curve: As for the heavy solid curve but for the DFF-8-h scheme and with initial conditions extracted from the DFF-8-h data assimilation cycle.

4. Summary and conclusions

In this paper, we have examined the ability of a digital filter technique to eliminate high-frequency gravity-wave noise in the context of an operational global data assimilation system. Oscillations in time with periods typically less than 8 h in a short-term forecast were considered as undesirable noise.

As discussed by Lynch and Huang (1992) and Huang and Lynch (1993), we found the digital filter to be very flexible and easy to implement. Unlike their approach, which involves performing an adiabatic integration backward in time in order to produce a balanced state at the analysis time, we have examined a technique which we refer to as *digital filter finalization*. In the context of a 6-h intermittent data assimilation cycle, this involves filtering the noise in a time series produced from a direct, uninitialized, 12-h forecast in order to produce a noise-free model-state 6 h after the analysis time. Thus no adiabatic approximation is involved and diabatic effects are fully taken into account.

The performance of the digital filter finalization (DFF) with an 8-h cutoff was examined from different points of view. The DFF scheme was found to produce insignificant changes to a fully-developed model state. In contrast, the currently-operational adiabatic NNMI procedure (which for the first three vertical modes initializes those gravity modes with natural periods less than 8 h) had a significant impact on the zonal-mean meridional mass streamfunction and the surface pressure field.

The robustness of the method, that is its ability to construct a balanced state from unbalanced data, was also examined. An examination of the time behaviour of a two-day forecast starting from initial conditions produced with the DFF scheme demonstrated the absence of noise in the tropics and extra-tropics. The surface-pressure tendencies were synoptically correct.

Finally, the impact of the DFF procedure in a global data assimilation system was examined. In evaluations of data assimilation cycles against radiosonde data, the DFF scheme yielded slightly better results than the NNMI-8-h scheme. Examination of the time-mean 6-h forecast and analysis increments (ΔF and ΔA, respectively) in terms of zonal-mean meridional mass streamfunction also revealed slightly better performance of the DFF scheme, the analysis increments being somewhat smaller in the tropics.

For a good representation of tidal oscillations, it was found advantageous to reduce the cutoff of the DFF scheme to 6 h. In general, this modified DFF scheme performed as well as the original DFF scheme, and in fact better than the NNMI-8-h scheme with regard to the tidal oscillation. However, this scheme was not quite as effective in removing the gravity-wave noise and also exhibited a slight deterioration in analysis performance in the tropics.

Thus overall the DFF procedure performed very well in a global data assimilation system. It produced results very close to the adiabatic NNMI-8-h scheme, i.e., from a practical point of view there were no significant differences in performance. An additional 6 h of integration is required, however, as compared to the standard NNMI procedure. One way in which the DFF scheme could be improved would be to sharpen the response in order to remove all noise with periods of less than say 8 h, while still retaining the full amplitude of the semi-diurnal oscillation. Some of the trade-offs in designing optimal filters are discussed in Huang and Lynch (1993).

In this study, the term "balance" has been used rather loosely to mean a model-state free of gravity-wave noise. Another aspect of the problem is how to improve the balance for the slow time scales, i.e., those that are retained in the model. One aspect of this problem is the consistency between the humidity and vertical motion fields (e.g., Kasahara et al., 1994; Krishnamurti et al., 1993; Puri and Davidson, 1992). This is especially important in the tropics where imbalances can generate spurious convection which affects the slow time scales.

The flexibility of the digital filter makes it attractive for use in limited-area regional models, as in Lynch and Huang (1992). However, the validity of filtering high-frequency gravity modes in mesoscale models still needs to be examined. The digital filter can also be used to filter the acoustic modes, when today's hydrostatic NWP models are replaced by non-hydrostatic ones. Thus, it is an alternative to the normal mode approach suggested by Daley (1988).

5. Acknowledgements

We thank Cécilien Charette for his help and suggestions during the course of this study.

6. Note added in proof

It was brought to our attention by one of the reviewers that the following related study was in press: Huang, X.-Y., Cederskov, A. and Kallen, E. 1994. A comparison between digital filtering initialization and nonlinear normal-mode initialization in a data assimilation system. *Mon. Wea. Rev.* **122**.

7. Appendix

The impact of adiabatic-NNMI with a 24-h cutoff period

As initially implemented in the CMC global data assimilation system, the adiabatic Machenhauer NNMI scheme was applied to the external and first two internal modes, for those gravity modes having natural periods less than 24 h. Based on preliminary results of this study, this cutoff period was reduced to 8 h in June 1993. We consider here the impact of a 24-h cutoff period on a balanced model state.

Fig. 10 shows the structure of the zonal-mean meridional mass streamfunction present in the control run at time τ (upper panel) and the *changes* due to applying the NNMI scheme at time τ using a cutoff period of 24 h (lower panel). Positive (negative) contours correspond to a counterclockwise (clockwise) circulation. These changes are much larger than with an 8-h cutoff (Fig. 2) and produce a weaker Hadley cell as compared to the control.

Examination of the amplitude of the divergent wind V_d for the control integration at time τ showed that it had maximum intensity at the level $\sigma = 0.190$. Values exceeding 10 m s^{-1} (and with

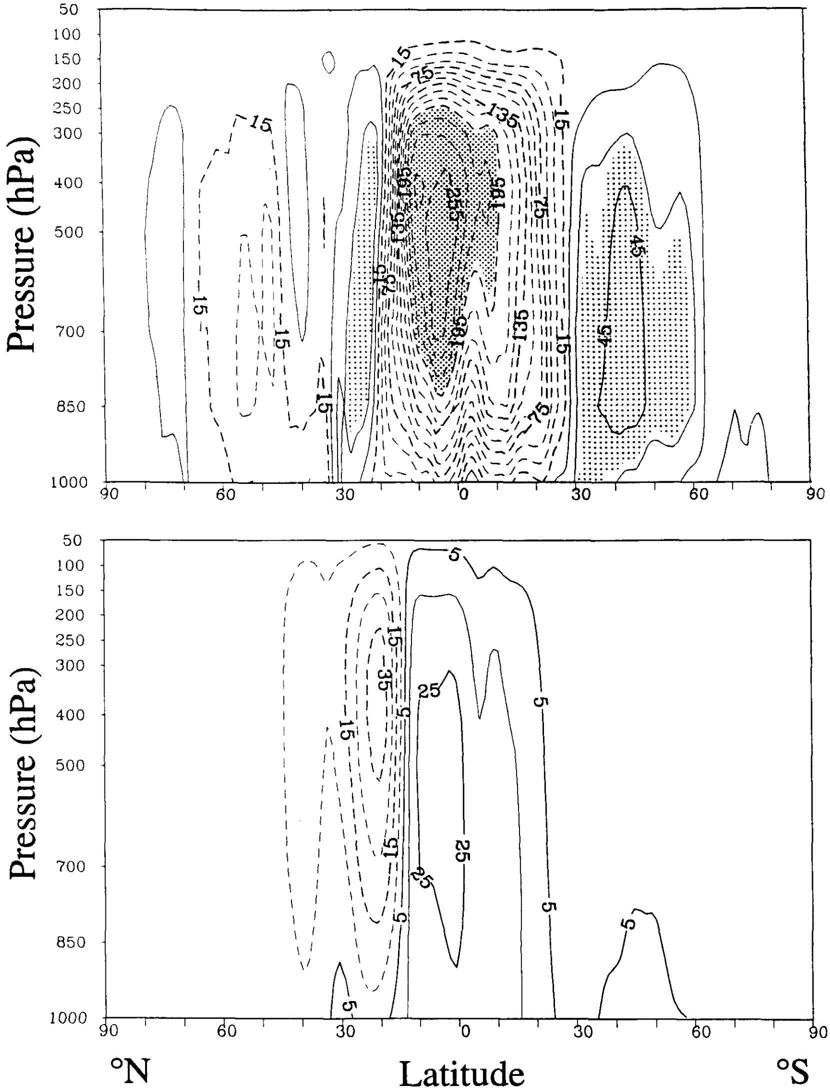

Fig. 10. Upper panel: the zonal-mean meridional mass streamfunction for the control integration at time τ. Contours are in units of 20×10^9 kg s^{-1}. Light stippling denotes regions greater than 30×10^9 kg s^{-1}. Heavy stippling denotes regions less than -200×10^9 kg s^{-1}. Lower panel: Changes to the meridional streamfunction for the control integration at time $t = \tau$ due to NNMI with a 24-h cutoff period. Contour interval is 10×10^9 kg s^{-1}.

maxima of about 15 m s^{-1}) appeared over the tropical region where convective forcing is a dominant effect. Fig. 11 shows the amplitude of the change in V_d at time τ produced by the NNMI scheme with a 24-h cutoff period. The maximum value (3.5 m s^{-1}) appears in the tropics. These changes can be considered as significant since they are comparable to the estimated analysis error at that level (Hollingsworth et al., 1989). A 48-h cutoff period produced changes of the same order of magnitude as the field itself (result not shown), consistent with the results of ER. Most of the amplitude of change appears for gravity modes with periods greater than 24 h.

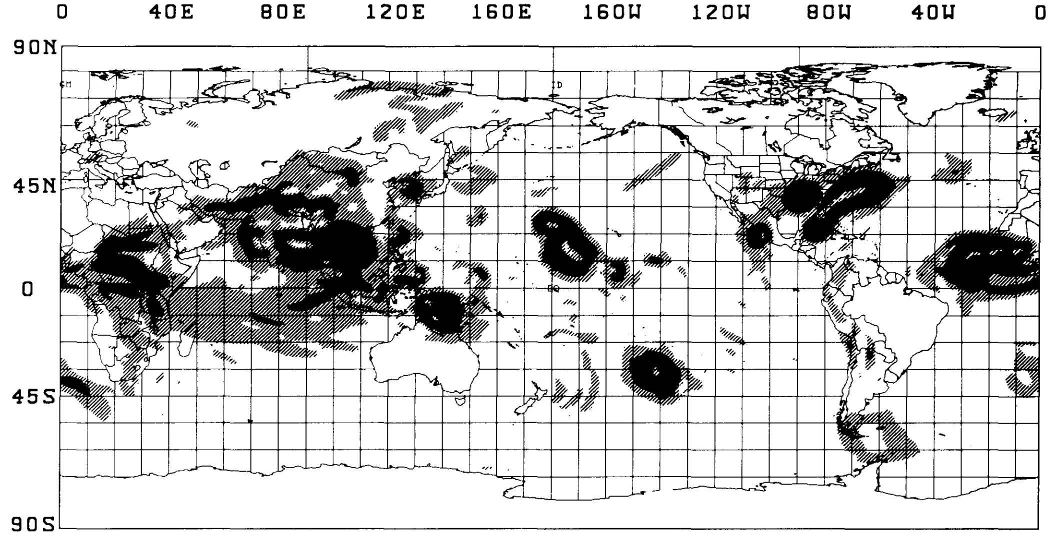

Fig. 11. Changes to V_d at time τ at $\sigma = 0.190$ for the NNMI scheme with a 24-h cutoff period. Light (heavy) stippling for values greater than 1 (2) m s^{-1} (respectively).

Fig. 12 shows the same type of field as Fig. 3 but using the NNMI-24-h scheme. It shows a zonal wavenumber two pattern with an amplitude of almost 2 hPa, i.e., the adiabatic NNMI scheme with a 24-h cutoff largely eliminates the semi-diurnal tide present in the thermally-forced circulation of the model. This deficiency with a 24-h cutoff can also be seen in Fig. 13. It can be seen that it takes 15–20 h for the model to re-establish the tidal oscillation, in agreement with the 18-h spin-up time reported by BAL92 for a somewhat different NNMI scheme.

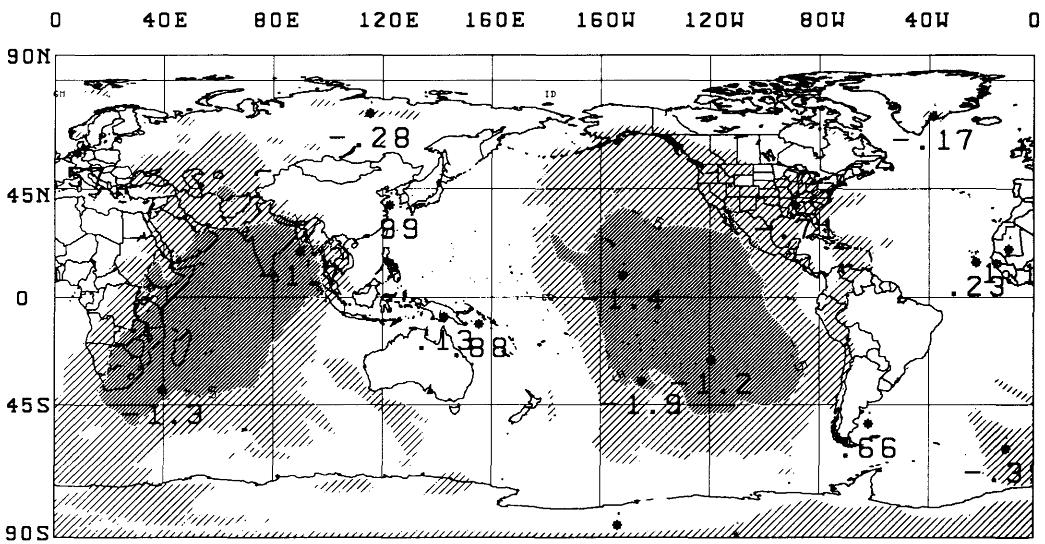

Fig. 12. As in Fig. 3 but using the NNMI scheme with a 24-h cutoff period. Light stippling is associated with values between 0 and −0.5 hPa, and heavy stippling with values less than −0.5 hPa.

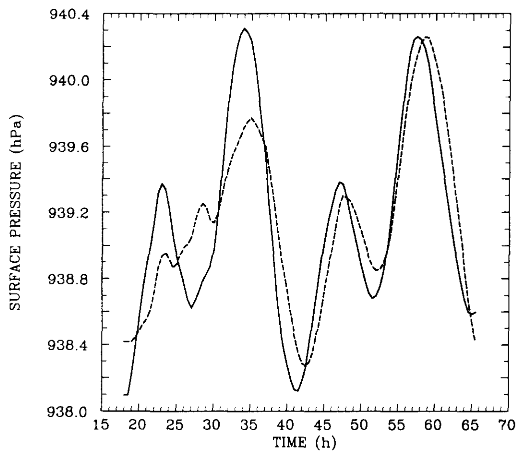

Fig. 13. As in Fig. 4, but the dashed curve is from initialized initial conditions using the NNMI-24-h scheme, while the solid curve is from initialized initial conditions using the NNMI-8-h scheme.

REFERENCES

Baer, F. and Tribbia, J. 1977. On complete filtering of gravity waves through nonlinear initialization. *Mon. Wea. Rev.* **105**, 1536–1539.

Ballish, B. A., Cao, X., Kalnay, E. and Kanamitsu, M. 1992. Incremental nonlinear normal-mode initialization. *Mon. Wea. Rev.* **120**, 1723–1734.

Béland, M. and Beaudoin, C. 1985. A global spectral model with a finite-element formulation for the vertical discretization: Adiabatic formulation. *Mon. Wea. Rev.* **113**, 1910–1919.

Bijlsma, S. J. and Hafkenscheid, L. M. 1986. Initialization of a limited area model: a comparison between the nonlinear normal mode and bounded derivative methods. *Mon. Wea. Rev.* **114**, 1445–1455.

Bourke, W. and McGregor, J. 1983. A nonlinear vertical mode initialization scheme for a limited area prediction model. *Mon. Wea. Rev.* **111**, 2285–2297.

Browning, G. and Kreiss, H.-O. 1982. Initialization of the shallow-water equations with open boundaries by the bounded derivative method. *Tellus* **34**, 334–351.

Côté, J., Roch, M., Staniforth, A. and Fillion, L. 1993. A variable-resolution semi-Lagrangian finite-element global model of the shallow-water equations. *Mon. Wea. Rev.* **121**, 231–243.

Courtier, P. and Talagrand, O. 1990. Variational assimilation of meteorological observations with the direct and adjoint shallow-water equations. *Tellus* **42A**, 531–549.

Daley, R. 1988. The normal modes of the spherical non-hydrostatic equations with applications to the filtering of acoustic modes. *Tellus* **40A**, 96–106.

Edelmann, W. 1972. Initial balancing and damping of gravitational oscillations for forecast models including the orography. *Beitr. Atmos. Phys.* **45**, 94–120.

Errico, R. M. 1984. Dynamic balance produced by a general circulation model. *Mon. Wea. Rev.* **112**, 2439–2454.

Errico, R. M. and Rasch, P. J. 1988. A comparison of various normal mode initialization schemes and the inclusion of diabatic processes. *Tellus* **40A**, 1–25.

Errico, R. M. and Bates, G. T. 1988. Implicit normal-mode initialization of the PSU/NCAR mesoscale model. *NCAR tech. note*, NCAR/TN − 312 + IA. 112 pp.

Errico, R. M., Barker, E. H. and Gelaro, R. 1988. A determination of balanced normal modes for two models. *Mon. Wea. Rev.* **116**, 2717–2734.

Errico, R. M. 1989. The degree of Machenhauer balance in a climate model. *Mon. Wea. Rev.* **117**, 2723–2733.

Gelaro, R. and Errico, R. 1993. The forcing and balance of zonally symmetric modes in a global model. *Mon. Wea. Rev.* **121**, 470–481.

Girard, C., Delage, Y., Mailhot, J., Garand, L., Bilodeau, B., Brunet, N. and Pellerin, G. 1991. Physical parameterization for the first Canadian global forecast model. Preprints, *9th AMS Conf. on Numerical weather prediction*, Denver, pp. 502–505.

Gustafsson, N. 1992. Use of a digital filter as a weak constraint in variational data assimilation. *Variational assimilation, with special emphasis on three-dimensional aspects.* ECMWF Seminar 1992, 327–338. [Available from the European Centre for Medium-Range Weather Forecasts, Shinfield Park, Reading RG2 9AX, England.]

Hamming, R. W. 1989. *Digital filters.* Prentice-Hall International, 284 pp.

Hollingsworth, A., Shaw, D. B., Lönnberg, P., Illari, L., Arpe, K. and Simmons, A. J. 1986. Monitoring of observation and analysis quality by a data assimilation system. *Mon. Wea. Rev.* **114**, 861–879.

Hollingsworth, A., Horn, J. and Uppala, S. 1989. Verification of FGGE assimilations of the tropical wind field: the effect of model and data bias. *Mon. Wea. Rev.* **117**, 1017–1038.

Huang, X.-Y. and Lynch, P. 1993. Diabatic digital-filtering initialization: Application to the HIRLAM model. *Mon. Wea. Rev.* **121**, 589–603.

Huang, X.-Y. and Sundqvist, H. 1993. Initialization of cloud water content and cloud cover for numerical prediction models. *Mon. Wea. Rev.* **121**, 2719–2726.

Juvanon du Vachat, R. 1992. Experiments with non-normal-mode initialization of a shallow-water limited-area model: Impact of relaxation, orography, and of an extended linearization including most of the β-terms. *Mon. Wea. Rev.* **120**,.2129–2155.

Kasahara, A., Mizzi, A. P. and Donner, L. J. 1994. Diabatic initialization for improvement in the tropical analysis of divergence and moisture using satellite radiometric imagery data. *Tellus* **46A**, 242–264.

Krishnamurti, T. N., Bedi, H. S. and Ingles, K. 1993. Physical initialization using SSM/I rainrates. *Tellus* **45A**, 247–269.

Lynch, P. and Huang, X.-Y. 1992. Initialization of the HIRLAM model using a digital filter. *Mon. Wea. Rev.* **120**, 1019–1034.

Machenhauer, B. 1977. On the dynamics of gravity oscillations in a shallow-water model, with application to normal mode initialization. *Contrib. Atmos. Phys.* **50**, 253–271.

Mitchell, H. L., Charette, C., Lambert, S. J., Hallé, J. and Chouinard, C. 1993. The Canadian global data assimilation system: description and evaluation. *Mon. Wea. Rev.* **121**, 1467–1492.

Parrish, D. F. and Derber, J. C. 1992. The National Meteorological Center's spectral statistical-interpolation analysis system. *Mon. Wea. Rev.* **120**, 1747–1763.

Puri, K. and Davidson, N. E. 1992. The use of infrared satellite cloud imagery data as proxy data for moisture and diabatic heating in data assimilation. *Mon. Wea. Rev.* **120**, 2329–2341.

Ritchie, H. 1991. Application of the semi-Lagrangian method to a multilevel spectral primitive-equations model. *Q. J. R. Meteorol. Soc.* **117**, 91–106.

Staniforth, A. N. and Daley, R. 1977. A finite-element formulation for the vertical discretization of sigma-coordinate primitive equation models. *Mon. Wea. Rev.* **105**, 1108–1118.

Temperton, C. 1988. Implicit normal mode initialization. *Mon. Wea. Rev.* **116**, 1013–1031.

Temperton, C. and Williamson, D. L. 1979. Normal mode initialization for a multilevel grid-point model. *ECMWF Tech. Rep. no. 11*, Shinfield Park, Reading, Berkshire RG2 9AX, UK, 91 pp.

Temperton, C. 1989. Implicit normal mode initialization for spectral models. *Mon. Wea. Rev.* **117**, 436–451.

Temperton, C. and Roch, M. 1991. Implicit normal mode initialization for an operational regional model. *Mon. Wea. Rev.* **120**, 667–677.

Thépaut, J. N. and Courtier, P. 1991. Four-dimensional variational data assimilation using the adjoint of a multilevel primitive equation model. *Q. J. R. Meteorol. Soc.* **117**, 1225–1254.

Thépaut, J. N., Vasiljevic, D., Courtier, P. and Pailleux, J. 1993. Variational assimilation of conventional meteorological observations with a multilevel primitive-equation model. *Q. J. R. Meteorol. Soc.* **119**, 153–186.

Wergen, W. 1989. Normal mode initialization and atmospheric tides. *Q. J. R. Meteorol. Soc.* **115**, 535–545.